

# Dual control cell reaction ensemble molecular dynamics: A method for simulations of reactions and adsorption in porous materials

Martin Lísal<sup>a)</sup>

*E. Hála Laboratory of Thermodynamics, Institute of Chemical Process Fundamentals, Academy of Sciences of the Czech Republic, 165 02 Prague 6-Suchbát, Czech Republic and Department of Physics, J. E. Purkyně University, 400 96 Ustí n. Lab., Czech Republic*

John K. Brennan

*U.S. Army Research Laboratory, Weapons and Materials Research Directorate, Aberdeen Proving Ground, Maryland 21005-5066*

William R. Smith

*Faculty of Science, University of Ontario Institute of Technology, 2000 Simcoe St. N., Oshawa ON L1H7K4, Canada*

Flor R. Siperstein

*Departament d'Enginyeria Química, ETSEQ, Universitat Rovira i Virgili, Avinguda dels Països Catalans, 26. 43007 Tarragona, Spain*

(Received 16 March 2004; accepted 21 June 2004)

We present a simulation tool to study fluid mixtures that are simultaneously chemically reacting and adsorbing in a porous material. The method is a combination of the reaction ensemble Monte Carlo method and the dual control volume grand canonical molecular dynamics technique. The method, termed the dual control cell reaction ensemble molecular dynamics method, allows for the calculation of both equilibrium and nonequilibrium transport properties in porous materials such as diffusion coefficients, permeability, and mass flux. Control cells, which are in direct physical contact with the porous solid, are used to maintain the desired reaction and flow conditions for the system. The simulation setup closely mimics an actual experimental system in which the thermodynamic and flow parameters are precisely controlled. We present an application of the method to the dry reforming of methane reaction within a nanoscale reactor model in the presence of a semipermeable membrane that was modeled as a porous material similar to silicalite. We studied the effects of the membrane structure and porosity on the reaction species permeability by considering three different membrane models. We also studied the effects of an imposed pressure gradient across the membrane on the mass flux of the reaction species. Conversion of syngas ( $H_2/CO$ ) increased significantly in all the nanoscale membrane reactor models considered. A brief discussion of further potential applications is also presented. © 2004 American Institute of Physics. [DOI: 10.1063/1.1782031]

## I. INTRODUCTION

With the rapid growth of nanotechnology and the invention of various nanomaterials, some of these materials have been proposed as vehicles for nanochemical devices such as nanoscale reactors and nanoscale membrane reactors.<sup>1</sup> However, development of these applications is impossible without fundamental knowledge of reaction, adsorption, and transport mechanisms in the nanoporous materials.

It is well established that confinement brings about drastic changes in the thermodynamics properties of fluids such as narrowing of the coexistence curve, lowering of the pore critical temperature, or increasing the average pore densities; for a comprehensive review see Ref. 2. Confinement also influences chemical reaction equilibrium. For example, gen-

erally the pore phase has a higher density than the corresponding bulk phase; this results in an increase in yield for reactions in which there is a decrease in the total number of moles (Le Chatellier's principle). Further, some components of the reaction mixture are selectively adsorbed on the solid surfaces, subsequently affecting the reaction equilibrium. Finally, molecular orientations can be strongly influenced by proximity to a solid surface which also can shift the reaction equilibrium from the bulk phase equilibrium. The effects of confinement on reaction equilibria were already studied by Turner *et al.*<sup>3-5</sup> for several realistic, reversible reactions in carbon micropores and carbon nanotubes, and by Borówko *et al.*<sup>6,7</sup> for model, reversible reactions in slitlike pores.

These authors employed the reaction ensemble Monte Carlo (REMC) simulation technique<sup>8-10</sup> that enables us to directly simulate equilibrium properties of chemically reacting systems. The method requires only a knowledge of the reaction species intermolecular potentials and their ideal-gas properties, in addition to specification of the system stoichi-

<sup>a)</sup>Author to whom correspondence should be addressed. Present address: E. Hála Laboratory of Thermodynamics, Institute of Chemical Process Fundamentals, Academy of Sciences of the Czech Republic, Rozvojová 135, 165 02 Prague 6-Suchbát, Czech Republic.

ometry and thermodynamic constraints. Recently, we proposed a combination of the REMC method with the molecular dynamics (MD) technique.<sup>11</sup> The method, termed the reaction ensemble molecular dynamics (RxMD) method, uses a combination of stochastic and dynamic simulation steps, allowing for the simulation of both thermodynamic and transport properties. The method couples a MD system (dynamic cell) to a reaction mixture reservoir (control cell) that is formulated upon the REMC method. Thermodynamic and transport properties are calculated in the dynamic cell by using a canonical MD simulation method. The RxMD method is analogous to the grand canonical molecular dynamics (GCMD) technique of Papadopoulou *et al.*<sup>12</sup> The accuracy and stability of the RxMD method was assessed by considering the ammonia synthesis reaction,  $N_2 + 3H_2 \rightleftharpoons 2NH_3$ .

Confinement also influences the transport properties of fluid particles inside the nanoporous materials. Physical space restrictions based on the fluid particle size or geometry may limit flow of particles through particular pores in the material. Furthermore, attraction of the pore surface, i.e., physisorption may play a critical role. Even further complicating the matters, fluid particles may chemisorb. In addition to phenomena occurring between fluid particles and the pore surface, behavior in the porous material becomes increasingly more complex if chemical reactions occur between fluid particles.

Confinement contributes significantly to the thermodynamic and transport properties if reactions and separation occur simultaneously in the nanoporous materials. Consider, for example, two voids in a nanoporous material separated by a semipermeable membrane with the elementary reversible reaction



occurring in one void only. If the membrane is permeable to product  $D$  only and the partial pressure of  $D$  on the permeate side of the membrane is lower than the partial pressure of  $D$  on the reaction side of the membrane then the separation process produces a flow of product  $D$  across the membrane. The removal of  $D$  from the “reaction” void via the separation function of the membrane has the following effects on the reaction shown in Eq. (1): (i) the reaction equilibrium condition is shifted to the right resulting in a higher conversion of reactants  $A$  and  $B$  to products  $C$  and  $D$ ; (ii) if there is an undesirable side reaction, e.g., that fouls a catalyst by a side product, such as



occurring in the reaction void, then the separation of product  $D$  from the reaction mixture reduces the amount of reactant  $B$  to the side reaction, increasing the selectivity of conversion to product  $C$  (or  $D$ ).<sup>13</sup>

In this work, we propose a nonequilibrium MD method for the simulation of combined reaction and adsorption mechanisms in porous materials. This method is a combination of the REMC and RxMD methods, and the dual control volume GCMD (DCV-GCMD) technique. The REMC and RxMD methods predict the physical effects on chemical re-

action equilibria from such influences as solvation and confinement. In addition, the RxMD method predicts the effects of nonideal environments on the molecular transport properties of chemically reacting mixtures. The DCV-GCMD method was independently proposed by Heffelfinger and van Swol,<sup>14</sup> and MacElroy,<sup>15</sup> and was extensively employed for studies of transport phenomena in confined systems; see, e.g., Refs. 16 and 17, and references therein.

We term the nonequilibrium simulation method the dual control cell reaction ensemble molecular dynamics (DCC-RxMD) method. The DCC-RxMD method allows for the simulation of the thermodynamic and transport properties of fluids in porous materials where reaction and adsorption is occurring simultaneously. Fluid particles move through the simulation cell via MD,<sup>18</sup> chemical reactions occur via the REMC method, and fluid transport (occurring as a result of an imposed pressure gradient between adjacent pores) via the grand canonical Monte Carlo (GCMC) method.<sup>19</sup>

We apply the DCC-RxMD method to study reactions and separations in a model of a nanoscale membrane reactor for dry reforming of methane. Dry reforming of methane is an important industrial process for producing syngas ( $H_2/CO$ ) that utilizes membrane technology.<sup>20</sup> We examine the effects of the membrane structure and porosity on the reaction species permeability by considering three different membrane models. We also examine the effects of an imposed pressure gradient across the membrane on the mass flux of the reaction species and reaction conversion.

The paper is organized as follows: Derivation and general computational considerations of the DCC-RxMD methodology are presented in Sec. II. Section III describes an illustrative application of the DCC-RxMD method for simulation of a multicomponent system in which both a chemical reaction (dry reforming of methane) and physisorption is occurring within a nanoporous solid. In addition, the technical details of this application of the DCC-RxMD methodology are given. Section IV presents and discusses DCC-RxMD results together with DCV-GCMD simulations for both the pure fluids and equimolar mixtures of the reaction components ( $CH_4$ ,  $CO_2$ ,  $H_2$ ,  $CO$ ). Section V contains our conclusions including a brief discussion of further potential applications of the DCC-RxMD method.

## II. SIMULATION METHODOLOGY

A molecular simulation method to study reactions and adsorption in porous materials is presented. The method uses a combination of stochastic and dynamic simulation steps, allowing for the simulation of both thermodynamic and transport properties. The method couples a MD system (dynamic cell) to reaction and nonreaction mixture reservoirs (control cells) that are formulated upon the REMC method<sup>8–10</sup> and GCMC method,<sup>19</sup> hence the term dual control cell reaction ensemble molecular dynamics (DCC-RxMD) method. The control cells are in direct contact with the dynamic cell and the particles are able to move freely between the cells. Transport properties are calculated in the dynamic cell by using a MD simulation method.<sup>18</sup> REMC forward and reverse reaction steps, and GCMC particle insertion and deletion steps are performed in the control cells

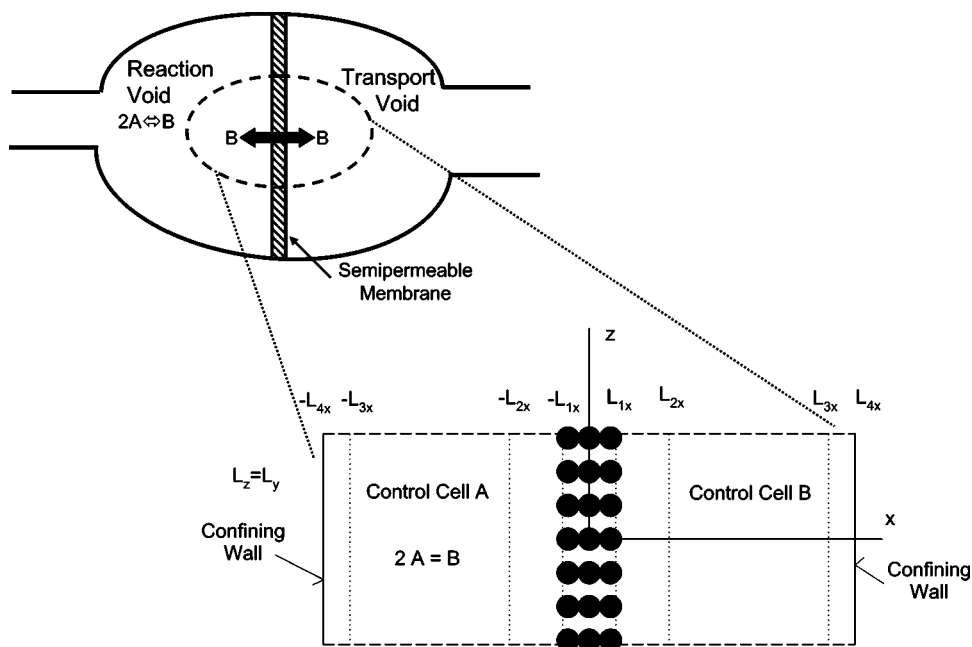
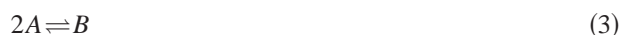


FIG. 1. Schematic of a nanoscale membrane reactor model made up of a reaction void and a transport void separated by a semipermeable membrane. A model reaction  $2A \rightleftharpoons B$  takes place in the reaction void while component  $B$  is separated via the semipermeable membrane. Enlargement shows schematic of the corresponding DCC-RxMD simulation setup. Periodic boundary conditions, applied in both the  $y$  and  $z$  directions, are omitted in the  $x$  direction due to the presence of repulsive confining walls (in the  $yz$  plane) at each end of the simulation setup.

only, while MD steps are performed in both the dynamic cell and the control cells. The control cells, which act as sink and source reservoirs, are maintained at explicitly defined and controlled gradient conditions, e.g., a pressure gradient. The DCC-RxMD method is analogous to the DCV-GCMD method;<sup>14,15</sup> all of which simulate conditions that directly relate to real, open systems. Computational details will be addressed below but first we illustrate the overall setup of the method.

Consider a nanoporous material containing a system of “nanomembrane reactors.” Each nanomembrane reactor is made up of two adjacent voids separated by a semipermeable membrane. One of the voids acts as a “nanoreactor” in which, for example, the model reaction



is occurring. We term this void the *reaction* void. The accompanying void in the nanomembrane reactor, termed the *transport* void, maintains a pressure gradient across the membrane. We further assume that the membrane separating the reaction and transport voids is not permeable to all molecular components. For example, in the model system of Eq. (3), suppose the membrane is permeable to component  $B$  only. For such a case, a difference in the partial pressures of component  $B$  in the reaction and transport voids results in a flux of component  $B$  through the membrane. A schematic of the nanomembrane reactor model made up of the reaction and transport voids separated by a semipermeable membrane is presented in Fig. 1. The nanomembrane reactor model is analogous to the slitpore model<sup>21</sup> which assumes that the nanomembrane reactor model is taken as representative of all nanomembrane reactors in the porous material. The effect of pore connectivity can be readily involved by considering a combination of connected nanomembrane reactor models.

To mimic reaction and adsorption mechanisms in such a nanoscale membrane reactor model, we consider a DCC-RxMD simulation box as shown in the enlargement of Fig. 1.

A membrane of thickness  $\delta = 2L_{1x}$  is placed at the center of the simulation box. The left-hand side of the simulation box (from  $-L_{1x}$  to  $-L_{4x}$ ) with control cell (CC) A (from  $-L_{2x}$  to  $-L_{3x}$ ) corresponds to a reaction void while the right-hand side of the simulation box (from  $L_{1x}$  to  $L_{4x}$ ) with CC B (from  $L_{2x}$  to  $L_{3x}$ ) corresponds to a transport void. Box lengths in the  $y$  and  $z$  directions are denoted by  $L_y$  and  $L_z$ , respectively. For simplicity, we considered that both CC A and CC B are of the same size and are positioned symmetrically with respect to the  $yz$  plane at  $x=0$ . We impose periodic boundary conditions in both the  $y$  and  $z$  directions since we assume that the sizes of the reaction and transport voids in these directions are much larger than the membrane thickness. To limit the size of the simulation setup in the  $x$  direction, repulsive confining walls are placed at the end of the simulation box. The size of the simulation box in the  $x$  direction must be sufficiently large to ensure that these confining-wall boundaries have negligible effect on the calculated fluid properties. The alternative to including confining-wall boundaries is to allow the fluid particles to leave the simulation box at the boundaries. Use of either the confining-wall boundaries or open-end boundaries give the same simulation results.<sup>15,22</sup> An alternative scenario is possible here. For example, one can consider a DCC-RxMD simulation box with two confining walls located in the  $z$  direction at a distance  $L_z$  apart without confining walls in the  $x$  direction.<sup>22</sup> In this scenario, confinement effects in the  $z$  direction are also considered important.

In either scenario, the DCC-RxMD simulation proceeds as follows. After  $n_{MD}$  MD steps, the system is frozen, i.e., particle positions are held fixed, and we perform  $n_{REMC}$  forward and reverse reaction steps in CC A, and  $n_{GCMC}$  particle creation and destruction steps in CC B. Both the REMC and GCMC algorithms require insertion of particles into the CCs. The velocities for such particles are assigned from a Maxwell-Boltzmann distribution corresponding to the speci-

fied system temperature.<sup>11,12</sup> Values of  $n_{\text{MD}}$ ,  $n_{\text{REMC}}$ , and  $n_{\text{GCMC}}$  must be chosen appropriately to maintain reaction equilibrium in CC A, constant chemical potentials in CC B, and reasonable transport rates at the boundaries between the CCs and the membrane region (the dynamic cell).

### A. Isothermal molecular dynamics

Trajectories of fluid particles within the entire DCC-RxMD simulation volume are generated by the MD simulation method.<sup>18</sup> The imposed pressure gradient across the membrane (a difference between pressures in CC A and CC B) produces heat that must be removed to maintain isothermal transport. Removal of the heat can be achieved by keeping the kinetic energy of the system  $E_k$  constant during MD steps.<sup>23</sup>  $E_k$  is defined in terms of  $\Delta\mathbf{p}_{i,l} = \mathbf{p}_{i,l} - \mathbf{p}_l$ , the relative momenta of particles with respect to the streaming momentum per particle for each of components  $l$ ,  $\mathbf{p}_l$ , evaluated as

$$\mathbf{p}_l = \frac{1}{N_l} \sum_{i=1}^{N_l} \mathbf{p}_{i,l}. \quad (4)$$

In Eq. (4),  $N_l$  is the number of particles of component  $l$  in the system and  $\mathbf{p}_{i,l}$  is the momentum of particle  $i$  for component  $l$ . The kinetic energy constraint for the system will be satisfied<sup>24</sup> if

$$\frac{dE_k}{dt} = \frac{1}{2} \frac{d}{dt} \left[ \sum_{l=1}^c \frac{1}{m_l} \sum_{i=1}^{N_l} (\Delta\mathbf{p}_{i,l})^2 \right] = 0, \quad (5)$$

where  $t$  is the time,  $m_l$  is the mass of component  $l$ , and  $c$  is the total number of components in the system. A set of equations of motion for the MD subject to the kinetic energy constraint given by Eq. (5) is<sup>25</sup>

$$\frac{d\mathbf{r}_{i,l}}{dt} = \frac{\mathbf{p}_{i,l}}{m_l}, \quad (6)$$

$$\frac{d\mathbf{p}_{i,l}}{dt} = \mathbf{f}_{i,l} - \alpha(\Delta\mathbf{p}_{i,l}), \quad (7)$$

where  $\mathbf{r}_{i,l}$  is the position of particle  $i$  for component  $l$  and  $\mathbf{f}_{i,l}$  is the force on such a particle.  $\alpha$  is computed from Eq. (5) as<sup>26</sup>

$$\alpha = \frac{\sum_{l=1}^c \frac{1}{m_l} \sum_{i=1}^{N_l} (\mathbf{f}_{i,l} \cdot \Delta\mathbf{p}_{i,l})}{\sum_{l=1}^c \frac{1}{m_l} \sum_{i=1}^{N_l} (\Delta\mathbf{p}_{i,l} \cdot \Delta\mathbf{p}_{i,l})} \quad (8)$$

$$= \frac{\frac{1}{2} \sum_{l=1}^c \frac{1}{m_l} \sum_{i=1}^{N_l} (\mathbf{f}_{i,l} \cdot \Delta\mathbf{p}_{i,l})}{E_k}. \quad (9)$$

The equations of motion for the isothermal MD method, Eqs. (6) and (7), were solved by the “leap-frog” version of the Verlet algorithm.<sup>26</sup> The algorithm starts with Eq. (7) by evaluating the unconstrained relative momenta  $\Delta\mathbf{p}_{i,l}^{un}$  at time  $t$ ,

$$\Delta\mathbf{p}_{i,l}^{un}(t) = \Delta\mathbf{p}_{i,l}(t - \Delta t/2) + \frac{\Delta t}{2} [\mathbf{f}_{i,l}(t) - \mathbf{f}_l(t)], \quad (10)$$

where  $\Delta t$  is the time step and

$$\mathbf{f}_l = \frac{1}{N_l} \sum_{i=1}^{N_l} \mathbf{f}_{i,l}. \quad (11)$$

$\Delta\mathbf{p}_{i,l}^{un}(t)$  is then used to compute an instantaneous temperature of the system  $\mathcal{T}(t)$  from the relation

$$\frac{F}{2} k_B \mathcal{T}(t) = \frac{1}{2} \sum_{l=1}^c \frac{1}{m_l} \sum_{i=1}^{N_l} (\Delta\mathbf{p}_{i,l}^{un})^2, \quad (12)$$

where  $F = 3(\sum_{l=1}^c N_l) - 1$  is the total number of degrees of freedom for the system and  $k_B$  is the Boltzmann's constant.  $\mathcal{T}(t)$  and the specified system temperature  $T$  are used to evaluate the constant  $\beta$  defined as

$$\beta = \sqrt{\frac{T}{\mathcal{T}(t)}}, \quad (13)$$

where  $\beta$  is related to the constant  $\alpha$  [defined by Eqs. (8) and (9)] via

$$\beta = \frac{1}{1 + \alpha(\Delta t/2)}. \quad (14)$$

Having determined  $\beta$ , we are able to obtain  $\mathbf{p}_{i,l}$  at time  $t + \Delta t/2$  as

$$\mathbf{p}_{i,l}(t + \Delta t/2) = (2\beta - 1)\mathbf{p}_{i,l}(t - \Delta t/2) + 2(\beta - 1)\mathbf{p}_l(t - \Delta t/2) + \Delta t [\beta \mathbf{f}_{i,l}(t) + (1 - \beta)\mathbf{f}_l(t)]. \quad (15)$$

Finally,  $\mathbf{r}_{i,l}$  at time  $t + \Delta t$  is obtained from Eq. (6) as

$$\mathbf{r}_{i,l}(t + \Delta t) = \mathbf{r}_{i,l}(t) + \Delta t \frac{\mathbf{p}_{i,l}(t + \Delta t/2)}{m_l}. \quad (16)$$

### B. Reaction ensemble Monte Carlo

The REMC method<sup>8-10</sup> is a powerful simulation tool for studying chemically reacting mixtures. The method only requires inputting the intermolecular potentials and the ideal-gas properties for the reaction species that are present. Most notably, the method does not require a reactive-type potential that mimics bond breakage and formation.<sup>27,28</sup> The REMC method predicts the shift in equilibria of an ideal-gas phase reaction due to nonideal conditions such as high temperature and high pressure as well as nonideal surrounding environments such as solvents and pore walls. Reactions are simulated by performing forward and reverse reaction steps according to the REMC algorithm which guarantees that the reaction equilibrium criteria for a set of  $R$  linearly, independent chemical reactions,

$$\sum_{i=1}^c \nu_{ji} \mu_i = 0, \quad j = 1, 2, \dots, R, \quad (17)$$

are established.<sup>29</sup> In Eq. (17),  $\nu_{ji}$  is the stoichiometric coefficient of component  $l$  in chemical reaction  $j$  and  $\mu_l$  is its chemical potential. The reaction equilibrium condition for our model reaction, Eq. (3), in CC A (the reaction void) is then

$$\mu_B^A - 2\mu_A^A = 0, \quad (18)$$

where  $\mu_l^A$  is the chemical potential of component  $l$  in CC A. Forward and reverse reaction steps are accepted with probabilities

$$\min \left[ 1, \frac{\Gamma}{V_A} \frac{N_A^A(N_A^A - 1)}{N_B^A + 1} \exp \left( -\frac{\Delta U_A}{k_B T} \right) \right] \quad (19)$$

and

$$\min \left[ 1, \frac{V_A}{\Gamma} \frac{N_B^A}{(N_A^A + 1)(N_A^A + 2)} \exp \left( -\frac{\Delta U_A}{k_B T} \right) \right], \quad (20)$$

respectively. In Eqs. (19) and (20),  $V_A$  is the volume of CC A,  $\Gamma$  is the ideal-gas quantity defined as

$$\Gamma = \frac{k_B T}{P^0} K, \quad (21)$$

where  $P^0$  is the standard state pressure of 1 bar,  $K$  is the equilibrium constant,<sup>29</sup>  $N_l^A$  is the number of particles of component  $l$  in CC A, and  $\Delta U_A$  is the change in the configurational energy  $U$  due to forward and reverse reaction attempts in CC A.

### C. Imposed pressure gradient (GCMC)

In order to maintain a flux of particles through the membrane, we impose a pressure gradient across it. The pressure gradient is indirectly controlled by performing GCMC particle insertion and deletion steps in CC B (the transport void) only. According to the GCMC algorithm,<sup>19</sup> the chemical potential of component  $l$  in CC B,  $\mu_l^B$ , is chosen and the creation and destruction of a particle of component  $l$  is accepted with probabilities

$$\min \left[ 1, \frac{V_B q_l(T)}{N_l^B + 1} \exp \left( \frac{\mu_l^B}{k_B T} \right) \exp \left( -\frac{\Delta U_B}{k_B T} \right) \right] \quad (22)$$

and

$$\min \left[ 1, \frac{N_l^B}{V_B q_l(T)} \exp \left( -\frac{\mu_l^B}{k_B T} \right) \exp \left( -\frac{\Delta U_B}{k_B T} \right) \right], \quad (23)$$

respectively. In Eqs. (22) and (23),  $V_B$  is the volume of CC B,  $q_l(T)$  is the internal contribution of the partition function for component  $l$ ,  $N_l^B$  is the number of particles of component  $l$  in CC B, and  $\Delta U_B$  is the change in the configurational energy  $U$  due to creation and destruction attempts in CC B.

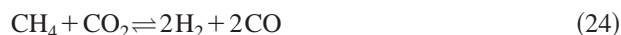
## III. ILLUSTRATIVE APPLICATION: A NANOSCALE MEMBRANE REACTOR MODEL

We applied the DCC-RxMD method to simulate a multicomponent system in which both a chemical reaction and physisorption is occurring within a nanoporous solid. We consider the dry reforming of methane reaction which is an important industrial process for producing syngas ( $H_2/CO$ ) from  $CH_4$  and  $CO_2$ .<sup>20</sup> We demonstrate how the reaction conversion is affected by separating out  $H_2$  from the reaction mixture via a semipermeable membrane. Below we provide

details of the reaction species models, membrane models, and further computational information specific to such the DCC-RxMD application.

### A. Reaction species potential models

We consider a nanoscale membrane reactor model (described in the preceding section, see also Fig. 1) in which the dry reforming reaction



occurs in the reaction void (CC A) and the membrane is (preferentially) permeable to  $H_2$ . A difference in the  $H_2$  partial pressures between the reaction and transport voids, i.e., between CC A and CC B will result in a  $H_2$  flux through the membrane. REMC forward and reverse reaction steps for the reaction shown in Eq. (24) are accepted with probabilities

$$\min \left[ 1, V_A^2 \Gamma \frac{N_{CH_4}^A N_{CO_2}^A}{(N_{H_2}^A + 1)(N_{H_2}^A + 2)(N_{CO}^A + 1)(N_{CO}^A + 2)} \times \exp \left( -\frac{\Delta U_A}{k_B T} \right) \right] \quad (25)$$

and

$$\min \left[ 1, \frac{1}{V_A^2 \Gamma} \frac{(N_{H_2}^A - 1)N_{H_2}^A(N_{CO}^A - 1)N_{CO}^A}{(N_{CH_4}^A + 1)(N_{CO_2}^A + 1)} \exp \left( -\frac{\Delta U_A}{k_B T} \right) \right], \quad (26)$$

respectively, where  $\Gamma$  is defined as

$$\Gamma = \left( \frac{P^0}{k_B T} \right)^2 K \quad (27)$$

and  $K$  is evaluated using the JANAF Tables.<sup>30</sup>

Components of the reaction system  $CH_4$ ,  $CO_2$ ,  $H_2$ , and  $CO$  are modeled as Lennard-Jones (LJ) spheres. The fluid-fluid interactions are approximated with a truncated-and-shifted LJ (TS-LJ) potential

$$u^{TS-LJ}(r_{ij}) = u^{LJ}(r_{ij}) - u_c^{LJ}, \quad r_{ij} \leq r_{c,ab} \quad (28)$$

$$= 0, \quad r_{ij} > r_{c,ab}, \quad (29)$$

where

$$u^{LJ}(r_{ij}) = 4\epsilon_{ab} \left[ \left( \frac{\sigma_{ab}}{r_{ij}} \right)^{12} - \left( \frac{\sigma_{ab}}{r_{ij}} \right)^6 \right], \quad (30)$$

$$u_c^{LJ} = 4\epsilon_{ab} \left[ \left( \frac{\sigma_{ab}}{r_{c,ab}} \right)^{12} - \left( \frac{\sigma_{ab}}{r_{c,ab}} \right)^6 \right]. \quad (31)$$

Here,  $r_{ij}$  is the distance between particle  $i$  for component  $a$  and particle  $j$  for component  $b$ ,  $\epsilon$ 's and  $\sigma$ 's are the effective LJ energy and size parameters, respectively, and  $r_{c,ab}$  is the spherical cutoff distance assigned to be  $r_{c,ab} = 3.5\sigma_{ab}$ . The  $\epsilon$ 's and  $\sigma$ 's for  $CH_4$ ,  $CO_2$ , and  $H_2$  were taken from Ref. 31, those for  $CO$  were taken from Ref. 32 and are listed in Table I. The cross-term LJ parameters were evaluated using the Lorentz-Berthelot combining rules,<sup>18</sup>

TABLE I. Effective LJ energy ( $\epsilon$ ) and size ( $\sigma$ ) parameters for CH<sub>4</sub>, CO<sub>2</sub>, H<sub>2</sub> (Ref. 31) and CO (Ref. 32) fluids, and membrane particles (Ref. 36).

Component	$\epsilon/k_B$ (K)	$\sigma$ (nm)
CH <sub>4</sub>	148.1	0.3810
CO <sub>2</sub>	225.3	0.3794
H <sub>2</sub>	38.0	0.290
CO	123.0	0.3662
Membrane	82.0	0.270

$$\epsilon_{ab} = \sqrt{\epsilon_{aa}\epsilon_{bb}}, \quad (32)$$

$$\sigma_{ab} = \frac{\sigma_{aa} + \sigma_{bb}}{2}. \quad (33)$$

Firouzi *et al.*<sup>33</sup> have confirmed that these LJ models for CH<sub>4</sub>, CO<sub>2</sub>, H<sub>2</sub>, and CO produced a phase diagram and thermodynamic properties which are in quantitative agreement with the experimental data, under both subcritical and supercritical conditions.

Fluid particles of component  $l$  interact with the repulsive confining walls  $w$  (see Fig. 1) via the TS-LJ potential with  $\epsilon_{lw}$ ,  $\sigma_{lw}$ , and  $r_{c,lw} = 2^{1/6}\sigma_{lw}$ . For simplicity, we use  $\epsilon_{lw} \equiv \epsilon_{ll}$  and  $\sigma_{lw} \equiv \sigma_{ll}$  since the confining walls have no direct influence on the transport in the membrane region and have only small effects on fluid properties in the portions of CCs adjacent to the confining walls.

## B. Membrane models

In order to increase the reaction conversion in our nanomembrane reactor model by separating out a particular product from the mixture, it is required that the membrane separating the reaction and transport voids be permeable to that particular product only. For the dry reforming of methane reaction considered here, we define our membrane model to be permeable to H<sub>2</sub> only while being impermeable to the remaining reaction species, namely, CH<sub>4</sub>, CO<sub>2</sub>, and CO. Since the dry reforming reaction is typically carried out at quite high temperatures, in general, the separation of mixture components via a membrane is based primarily on molecular sieving caused by the passage of smaller molecules of the mixture through the pores while the larger molecules are obstructed.<sup>34</sup> As evident in Table I, H<sub>2</sub> molecules are smaller than the CH<sub>4</sub>, CO<sub>2</sub>, and CO molecules. Hence, a characteristic size for the membrane pores should be greater than  $\sigma_{H_2}$  (to allow H<sub>2</sub> to permeate through the membrane) but yet less than or comparable to  $\sigma_{CH_4} \approx \sigma_{CO_2} \approx \sigma_{CO}$  (to obstruct CH<sub>4</sub>, CO<sub>2</sub>, and CO from permeating through the membrane).

We utilized two types of membrane models. The first model, proposed by Powles *et al.*,<sup>25,35</sup> defines membranes by several layers of LJ particles (characterized by the energy and size parameters  $\epsilon_m$  and  $\sigma_m$ , respectively) with a distance between layers equal to  $2^{1/6}\sigma_m$  (which corresponds to the LJ potential minimum). The particles in each layer are arranged in a face-centered cubic (fcc) structure. The layers are built by replicating a four-particle fcc primitive cell in the  $y$  and  $z$  directions. A two-dimensional schematic of a layer of particles for this model, termed the Powles' membrane

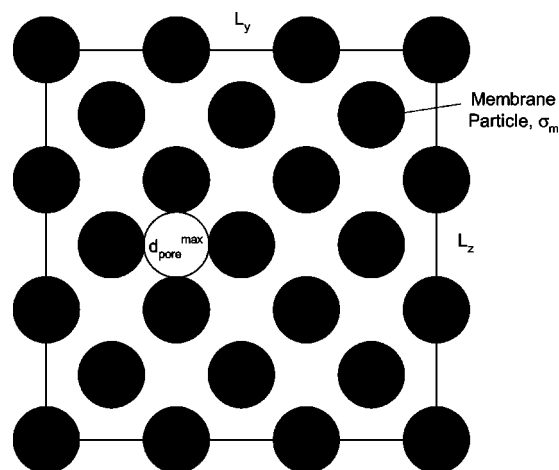


FIG. 2. Schematic of a fcc membrane layer for the Powles' membrane model discussed in text. The size of the particles making up the membrane is characterized by  $\sigma_m$ . An open circle of diameter  $d_{pore}^{max}$  indicates the maximum size of a membrane pore.

model (PM), is shown in Fig. 2. Also shown is the maximum allowable size  $d_{pore}^{max}$  for a pore in the membrane structure. Chosen values for  $\epsilon_m$  and  $\sigma_m$  correspond to silicalite molecules<sup>36</sup> and are listed in Table I. The membrane particles interact with fluid particles via the TS-LJ potential, Eqs. (28) and (29), and with the cross-term LJ parameters evaluated from the Lorentz-Berthelot combining rules, Eqs. (32) and (33). Powles' model generates membranes with well-defined structures comprising straight channels that are prototypical of zeolitic structures. We built two Powles' membranes and denote them PM1 and PM2. Both models consist of seven fcc layers but differ by their values of  $d_{pore}^{max}$ . PM1 has  $d_{pore}^{max} = 0.3253$  nm which corresponds to a membrane number density  $\rho_m = 21.728$  nm<sup>-3</sup> while PM2 is characterized by  $d_{pore}^{max} = 0.4104$  nm and  $\rho_m = 16.635$  nm<sup>-3</sup>. Geometric pore size distributions<sup>37</sup> (PSDs) for PM1 and PM2 are displayed in Fig. 3. As expected, Fig. 3 shows PSDs that are quite narrow with maximum peaks corresponding to  $d_{pore}^{max}$ .

The second type of membrane model used in this study comprises random configurations of nonoverlapping LJ spheres. The model, termed the random membrane model (RM), is generated from a canonical Monte Carlo simulation of hard spheres with a corresponding diameter of  $\sigma_m$ .<sup>38</sup> We built RMs with various PSDs in the volume  $2L_{1x} \times L_y \times L_z$  where the same value of  $L_{1x}$  as in PM1 and PM2 is used. We then chose one RM whose PSD peak is roughly at the same position as the PSD peak for PM2. The chosen RM has  $\rho_m = 15.156$  nm<sup>-3</sup> and its PSD is displayed in Fig. 3. Figure 3 shows that the PSD for the RM is substantially broader than that of PM2 due to the random arrangement of the membrane particles.

## C. Computational details

In addition to the DCC-RxMD simulations, we also carried out DCV-GCMD simulations for pure CH<sub>4</sub>, CO<sub>2</sub>, H<sub>2</sub>, and CO, and an equimolar mixture of CH<sub>4</sub>/CO<sub>2</sub>/H<sub>2</sub>/CO. In the DCV-GCMD simulations both CCs are used to maintain constant chemical potentials for the particular components.

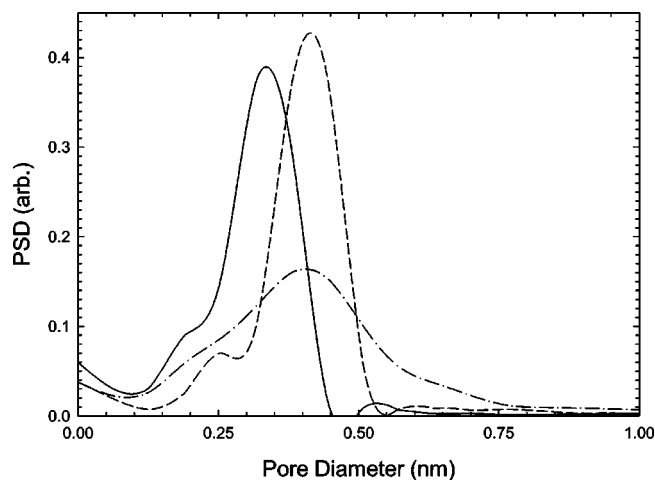


FIG. 3. Computed geometric pore size distributions (PSD) for the three membrane models: PM1 (—), PM2 (---), and RM (-·-·-·-). Units for the  $y$  coordinates are arbitrary.

Setting different values for the chemical potentials in CC  $A$  and CC  $B$  results in different pressures in these CCs. The imposed pressure gradient across the membrane causes a flux of fluid particles through the membrane. Hence, the DCV-GCMD simulations enable us to investigate properties of the membranes PM1, PM2, and RM independent of chemical reaction behavior. For the DCV-GCMD and DCC-RxMD simulation boxes, we used  $L_{1x}=L_{2x}=0.909\,066$  nm ( $L_{1x}=0.909\,066$  nm corresponds to seven membrane layers in PM1 and PM2),  $L_{3x}=18.288$  nm,  $L_{4x}=19.050$  nm, and  $L_y=L_z=9.525$  nm. Use of  $L_{1x}=L_{2x}$  (see Fig. 1) minimizes possible steric hindrance effects at the entrance of the membrane pores.<sup>39</sup>

After some preliminary test runs, we found that  $n_{MD}=10$ ,  $n_{REMC}=300$ , and  $n_{GCMD}=300$  are satisfactory values to properly maintain reaction equilibrium in CC  $A$ , constant chemical potentials in CC  $B$ , and reasonable transport rates at the boundaries between the CCs and the membrane region. Typically, there are 600 fluid particles in CC  $A$  and 10–500 fluid particles in CC  $B$ . Simulations were started with particles distributed in CC  $A$  and CC  $B$  only and no particles in the membrane region. We then carried out typically 0.25 ns simulation runs to achieve steady state. Subsequent production runs ranged from 1 ns for pure DCV-GCMD simulations to 2 ns for mixture DCV-GCMD and DCC-RxMD simulations, where  $\Delta t=3.438$  fs.

During the simulation we evaluated the excess internal energy  $u$ , number density  $\rho$ , pressure  $P$ , and compositions  $x_i^A$  and  $x_i^B$  of the mixtures in the CCs. The pressure was computed from the virial theorem.<sup>18</sup> To minimize the influence of the interfaces between the CCs and the membrane region as well as the effects of the confining walls on the adjacent portions of the CCs, fluid properties in the CCs were calculated in a predetermined interior portion of the CCs. More specifically, the fluid property calculations were applied only to molecules in CCs whose  $x$  coordinates were at a distance greater than  $\max\{r_{c,hw}\}_{l=1}^4$  from the CCs boundaries. We also calculated the molar flux through the membranes for component  $l$ ,  $J_l$ , and the permeability of compo-

nent  $l$ ,  $K_l$ .  $J_l$  was determined from the expression

$$J_l = \frac{N_l^{\text{LTR}} - N_l^{\text{RTL}}}{N_A A_{yz} N_{\text{MDsteps}} \Delta t} \quad (34)$$

and  $K_l$  was defined as

$$K_l = \frac{J_l^x}{\Delta P_l / \delta}. \quad (35)$$

In Eqs. (34) and (35),  $N_l^{\text{LTR}}$  and  $N_l^{\text{RTL}}$  are the net movement of particles for component  $l$  through the  $yz$  plane at  $x=0$  from left-to-right and from right-to-left, respectively,  $N_A$  is Avogadro's number,  $A_{yz}=L_y L_z$  is the  $yz$  area of the simulation box,  $N_{\text{MDsteps}}$  is the total number of isothermal MD steps, and  $\Delta P_l = x_l^A P_A - x_l^B P_B$  is the partial pressure difference for component  $l$ .

## IV. RESULTS AND DISCUSSIONS

### A. DCV-GCMD

Before presenting results for the increase of reaction conversion by separation of the  $H_2$  product from the reaction mixture of  $CH_4/CO_2/H_2/CO$  for the dry reforming reaction, we present results from DCV-GCMD simulations for the pure fluids and equimolar mixtures. The intent is to investigate the properties of the membrane models PM1, PM2, and RM independent of chemical reaction behavior. We performed all simulations at a typical temperature for the dry reforming reaction,  $T=1100$  K.<sup>20</sup>

#### 1. Pure fluids

In the DCV-GCMD simulations for pure  $CH_4$ ,  $CO_2$ ,  $H_2$ , and  $CO$ , we set  $\mu^A/(RT) = -4.039$  and varied  $\mu^B/(RT)$  from  $-4.308$  to  $-5.520$ ;  $R$  is the universal gas constant. This results in a pressure difference  $\Delta P = P_A - P_B$  ranging from 7 bars to 37 bars, where  $P_A \approx 48$  bars. Figure 4 presents  $J_l$  as a function of  $\Delta P$  for all three membrane models. Values of  $K_l$  for the membrane models did not show (within statistical uncertainties) dependence on  $\Delta P$ . Averaged  $K_l$  values are listed in Table II. Figure 4 and Table II show that only PM1 is, strictly speaking semipermeable, i.e., permeable to  $H_2$  and completely impermeable to  $CH_4$ ,  $CO_2$ , and  $CO$ . Both PM2 and RM exhibit very small yet undesirable permeabilities for  $CH_4$ ,  $CO_2$ , and  $CO$  in addition to substantial permeability for  $H_2$ . However, semipermeable membranes in industrial membrane reactors also exhibit small undesirable permeabilities for nonseparating components. In the cases of PM2 and RM, typical values of the molar fluxes for  $CH_4$ ,  $CO_2$ , and  $CO$  are one order smaller than the corresponding values of the molar flux for  $H_2$ . Similar behavior is exhibited for component permeabilities. Note that since  $\sigma_{CH_4} \approx \sigma_{CO_2} \approx \sigma_{CO}$  and since at  $T=1100$  K values of  $\epsilon$ 's have only a moderate influence on the transport properties,  $J_{CH_4} > J_{CO} > J_{CO_2}$  in the case of PM2 is primarily due to  $m_{CH_4} < m_{CO} < m_{CO_2}$ . In contrast to PM2 the effect of the different masses of the components on  $J_l$  is less pronounced for RM. This is due to the ability of the particles to pass more freely through the straight pores of PM2 as opposed to the contour pores of RM. Also note in Fig. 4 that at the same  $\Delta P$ , values of  $J_{H_2}$

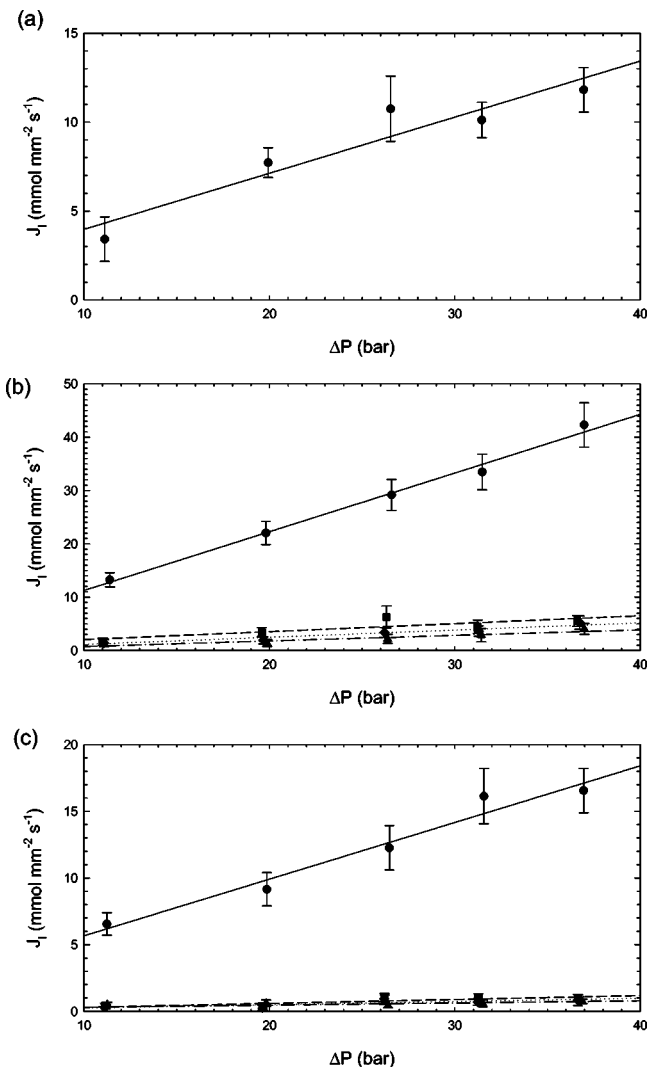


FIG. 4. Molar flux through the membrane models (a) PM1, (b) PM2, and (c) RM for component  $l$ ,  $J_l$ , as a function of the pressure difference  $\Delta P$  obtained from the DCV-GCMD simulations for pure  $\text{CH}_4$  (■),  $\text{CO}_2$  (▲),  $\text{H}_2$  (●), and  $\text{CO}$  (◆). Lines serve as a guide to the eye only.

in PM1 are about three times smaller than values of  $J_{\text{H}_2}$  in PM2. Further, values of  $J_{\text{H}_2}$  in PM2 are approximately two times larger than those found in RM. This behavior is a consequence of the well defined pore structure of PM2 whose PSD is much narrower compared to the PSD of RM.

Figure 5 shows typical density profiles for  $\text{H}_2$  across the membrane models PM1, PM2, and RM at  $\Delta P \approx 32$  bars. The high-pressure and low-pressure sides of the membrane correspond to  $\approx x = -1$  and  $1$  nm, respectively, implying a flux of  $\text{H}_2$  particles from left to right in Fig. 5. The vertical dotted lines denote the membrane model boundaries. The density profiles for PM1 and PM2 exhibit oscillatory character with minimums corresponding to the membrane layers and with maximums at positions between them. The density profile for RM decreases nearly monotonically from the high-pressure to low-pressure membrane sides due to the random configuration of membrane particles in RM. The behavior of the relative permeabilities of  $\text{H}_2$  for the different membrane models is reiterated in Fig. 5.

## 2. Equimolar mixtures

In the DCV-GCMD mixtures simulations, we set  $\{\mu_l^A/(RT)\}_{l=1}^4 = \{-5.385, -5.385, -5.385, -5.385\}$  and varied  $\{\mu_l^B/(RT)\}_{l=1}^4$  from  $\{-5.655, -5.655, -5.655, -5.655\}$  to  $\{-6.732, -6.732, -6.732, -6.732\}$  by keeping  $\mu_{\text{CH}_4}^B = \mu_{\text{CO}_2}^B = \mu_{\text{H}_2}^B = \mu_{\text{CO}}^B$ . This results in  $\Delta P$  ranging from 7 bars to 37 bars, where  $P_A \approx 50$  bars. At  $T = 1100$  K, mixtures in CC A and CC B are marginally nonideal and hence, the used values of  $\mu_l^A$  and  $\mu_l^B$  produce roughly equimolar mixture compositions in both CCs, i.e.,  $x_l^A \approx x_l^B \approx 0.25$ . Plots of  $J_l$  as a function of the partial pressure difference  $\Delta P_l$  for all three membrane models are given in Fig. 6. As in the case of pure fluids, values of  $K_l$  did not show (within statistical uncertainties) dependence on  $\Delta P_l$  (see Table II). From Fig. 6 and Table II we can draw similar conclusions about the dependence of the molar fluxes and permeabilities based on the relative membrane PSDs and structures. The notable difference being that the values of  $J_l$  for equimolar mixtures are smaller than corresponding values of  $J_l$  for pure fluids since  $\Delta P_l \approx 0.25\Delta P$ .

## B. DCC-RxMD

At  $T = 1100$  K and a bulk volume  $V \equiv V_A = (L_{3x} - L_{2x}) \times L_y \times L_z = 1576.71 \text{ nm}^3$ , both the REMC and RxMD predict the following bulk equilibrium properties of the reaction mixture  $\text{CH}_4/\text{CO}_2/\text{H}_2/\text{CO}$ :  $u = -0.057_{26} \text{ kJ mol}^{-1}$ ,  $P = 50.7_{11} \text{ bars}$ ,  $\rho = 0.3291_{184} \text{ nm}^{-3}$ ,  $x_{\text{CH}_4} = 0.222_{10}$ ,  $x_{\text{CO}_2} = 0.222_{10}$ ,  $x_{\text{H}_2} = 0.278_{10}$ , and  $x_{\text{CO}} = 0.278_{10}$ ; subscripts in numerical values denote the standard deviations in the last digits. Simulations were initiated with  $N_{\text{CH}_4}^{\text{ini}} = N_{\text{CO}_2}^{\text{ini}} = N_{\text{H}_2}^{\text{ini}} = N_{\text{CO}}^{\text{ini}} = 125$  molecules in the simulation box. At equilibrium, the total number of molecules in the bulk reaction system was  $N = \sum_{l=1}^c N_l = 520_5$ .

All DCC-RxMD simulations were started with  $N_{\text{CH}_4}^{\text{ini}} = N_{\text{CO}_2}^{\text{ini}} = N_{\text{H}_2}^{\text{ini}} = N_{\text{CO}}^{\text{ini}} = 125$  in CC A, i.e., with  $N_A^{\text{ini}} = 500$ . Values of  $\mu_l^B$  were chosen in such a way to obtain virtually pure  $\text{H}_2$  in CC B. This was achieved by setting  $\mu_{\text{CH}_4}^B/(RT) = \mu_{\text{CO}_2}^B/(RT) = \mu_{\text{CO}}^B/(RT) = -12.117$ . Values of  $\mu_{\text{H}_2}^B/(RT)$  were then varied from  $-4.712$  to  $-8.078$ . This results in  $\Delta P > 0$  but  $\Delta P_{\text{H}_2} < 0$  for  $\mu_{\text{H}_2}^B/(RT) > -5.25$  and  $\Delta P_{\text{H}_2} > 0$  otherwise. Note that the pressure in the reaction void decreases with the removal of  $\text{H}_2$  since the total number of particles decreases (see Figs. 7–9). For  $\Delta P_{\text{H}_2} < 0$ ,  $\text{H}_2$  flows from the transport void to the reaction void while for  $\Delta P_{\text{H}_2} > 0$ , there is a  $\text{H}_2$  flux from the reaction void to the transport void. Further,  $\mu_{\text{H}_2}^B/(RT) = -8.078$  produces nearly vacuum conditions in CC B, i.e., the equilibrium number of particles in CC B becomes very small and thus  $P_B \rightarrow 0$ . Hence, the value of  $\Delta P_{\text{H}_2}$  resulting from  $\mu_{\text{H}_2}^B/(RT) = -8.078$  corresponds roughly to the maximum achievable  $\Delta P_{\text{H}_2}$ .

Figures 7–9 show  $J_{\text{H}_2}$  and  $N_A/N_A^{\text{ini}}$ , and  $x_l^A$  as a function of  $\Delta P_{\text{H}_2}$  for all three membrane models. Note that  $x_l^A$  at  $\Delta P_{\text{H}_2} = 0$  corresponds to  $x_l^A$  of the bulk reaction system. We see from Figs. 7–9 that the maximal  $\Delta P_{\text{H}_2}$  [corresponding to  $\mu_{\text{H}_2}^B/(RT) = -8.078$ ] is directly related to values of

TABLE II. Permeabilities  $K_l$  obtained from the DCV-GCMD simulations of pure  $\text{CH}_4$ ,  $\text{CO}_2$ ,  $\text{H}_2$ , and  $\text{CO}$ , and an equimolar mixture of  $\text{CH}_4/\text{CO}_2/\text{H}_2/\text{CO}$  for all three membranes PM1, PM2, and RM. Subscripts in table values denote the standard deviations in the last digits.

Pure fluids				
Membrane	$K_{\text{CH}_4} \times 10^6$ (mmol bar <sup>-1</sup> mm <sup>-1</sup> s <sup>-1</sup> )	$K_{\text{CO}_2} \times 10^6$ (mmol bar <sup>-1</sup> mm <sup>-1</sup> s <sup>-1</sup> )	$K_{\text{H}_2} \times 10^6$ (mmol bar <sup>-1</sup> mm <sup>-1</sup> s <sup>-1</sup> )	$K_{\text{CO}} \times 10^6$ (mmol bar <sup>-1</sup> mm <sup>-1</sup> s <sup>-1</sup> )
PM1	0 <sub>9</sub>	0 <sub>9</sub>	400 <sub>50</sub>	15 <sub>15</sub>
PM2	200 <sub>40</sub>	77 <sub>55</sub>	1270 <sub>40</sub>	145 <sub>9</sub>
RM	35 <sub>9</sub>	35 <sub>20</sub>	570 <sub>60</sub>	35 <sub>9</sub>
Equimolar mixture				
Membrane	$K_{\text{CH}_4} \times 10^6$ (mmol bar <sup>-1</sup> mm <sup>-1</sup> s <sup>-1</sup> )	$K_{\text{CO}_2} \times 10^6$ (mmol bar <sup>-1</sup> mm <sup>-1</sup> s <sup>-1</sup> )	$K_{\text{H}_2} \times 10^6$ (mmol bar <sup>-1</sup> mm <sup>-1</sup> s <sup>-1</sup> )	$K_{\text{CO}} \times 10^6$ (mmol bar <sup>-1</sup> mm <sup>-1</sup> s <sup>-1</sup> )
PM1	9 <sub>9</sub>	0 <sub>9</sub>	450 <sub>60</sub>	0 <sub>9</sub>
PM2	180 <sub>9</sub>	95 <sub>25</sub>	1270 <sub>70</sub>	120 <sub>40</sub>
RM	25 <sub>30</sub>	20 <sub>20</sub>	575 <sub>120</sub>	35 <sub>25</sub>

$K_{\text{H}_2}$ : a membrane model with a larger  $K_{\text{H}_2}$  has a lower  $\Delta P_{\text{H}_2}$  (cf., e.g., the case of PM2 with  $K_{\text{H}_2} \approx 1270 \times 10^{-6}$  mmol bar<sup>-1</sup> mm<sup>-1</sup> s<sup>-1</sup> and maximal  $\Delta P_{\text{H}_2} \approx 3$  bars with the case of PM1 with  $K_{\text{H}_2} \approx 400 \times 10^{-6}$  mmol bar<sup>-1</sup> mm<sup>-1</sup> s<sup>-1</sup> and maximal  $\Delta P_{\text{H}_2} \approx 8$  bars). Also note that the upper portions of Figs. 7–9 show that the values of  $J_{\text{H}_2}$  corresponding to the maximal  $\Delta P_{\text{H}_2}$  are approximately the same. In contrast to these values of  $J_{\text{H}_2}$ , the values of  $N_A/N_A^{\text{ini}}$  at the maximal  $\Delta P_{\text{H}_2}$  differ significantly; they are lower for membranes with a higher  $K_{\text{H}_2}$ . Next note that compositions  $x_l^A$  as a function of  $\Delta P_{\text{H}_2}$  in the lower portions of Figs. 7–9 show that the compositions of reactants  $\text{CH}_4$  and  $\text{CO}_2$  decrease slowly with increasing  $\Delta P_{\text{H}_2}$  (except  $x_{\text{CH}_4}^A$  and  $x_{\text{CO}_2}^A$  close to the maximal  $\Delta P_{\text{H}_2}$  for PM2). The composition of the product

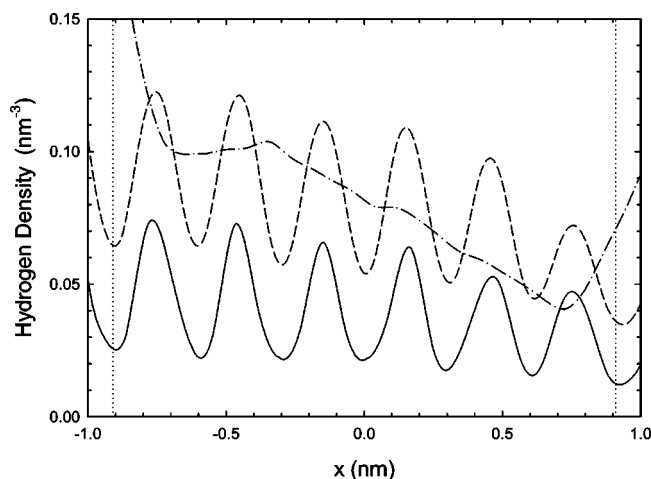


FIG. 5. Density profiles for  $\text{H}_2$  across the membrane models PM1 (—), PM2 (---), and RNM (-·-·-) at  $\Delta P \approx 32$  bars. The dotted lines denote the membrane boundaries.  $\text{H}_2$  molecules are flowing from left-to-right due to the imposed pressure gradient.

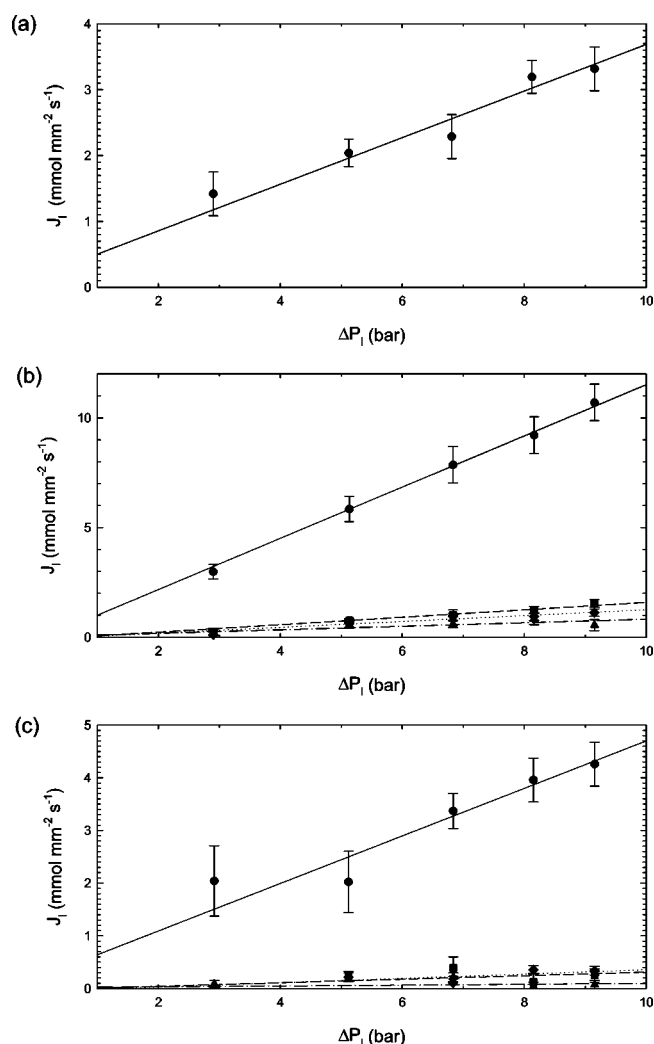


FIG. 6. Molar flux through the membrane models (a) PM1, (b) PM2, and (c) RM for component  $l$ ,  $J_l$ , as a function of the partial pressure difference  $\Delta P_l$  obtained from the DCV-GCMD simulations for equimolar mixtures of  $\text{CH}_4$  (■)/ $\text{CO}_2$  (▲)/ $\text{H}_2$  (●)/ $\text{CO}$  (◆). Lines serve as a guide to the eye only.

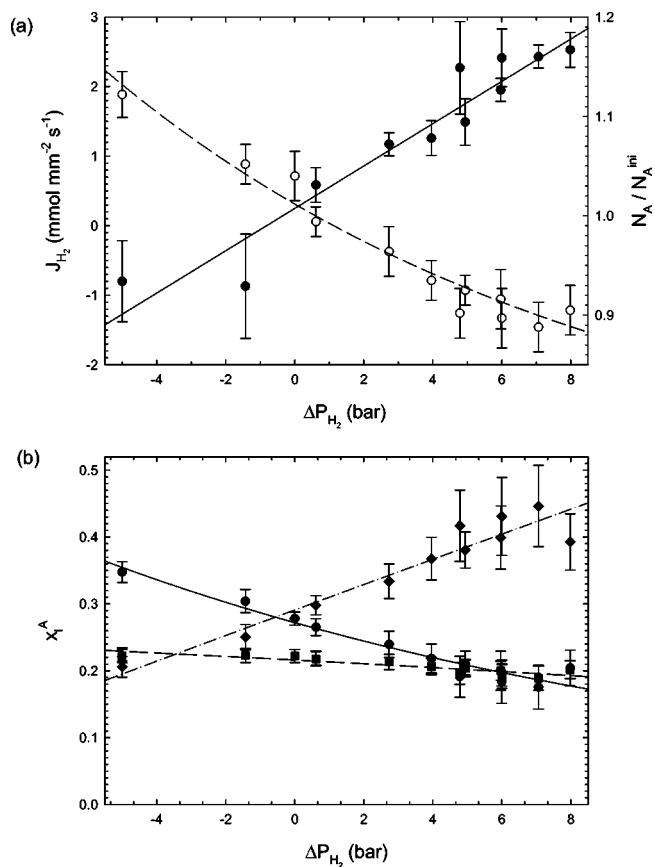


FIG. 7. (a) Hydrogen molar flux  $J_{H_2}$  (●) and  $N_A/N_A^{ini}$  (○) as a function of the hydrogen partial pressure difference  $\Delta P_{H_2}$ , and (b) the composition in the reaction void  $x_i^A$  (CH<sub>4</sub>, ■; H<sub>2</sub>, ●; CO, ◆) as a function of  $\Delta P_{H_2}$  in the case of PM1 obtained from the DCC-RxMD simulations. Due to identical initial compositions of CH<sub>4</sub> and CO<sub>2</sub>  $x_{CH_4}^A = x_{CO_2}^A$  within statistical uncertainties, therefore  $x_{CO_2}^A$  is not plotted. Lines serve as a guide to the eye only.

CO increases significantly with increasing  $\Delta P_{H_2}$ . At the maximal  $\Delta P_{H_2}$ ,  $x_{CO}^A$  is larger for membranes with a larger  $K_{H_2}$ . With respect to  $x_{CO}^A$  at  $\Delta P_{H_2} = 0$ , increases of  $x_{CO}^A$  at the maximal  $\Delta P_{H_2}$  are  $\sim 60\%$  for PM1,  $\sim 80\%$  for RM, and  $\sim 150\%$  for PM2.  $x_{H_2}^A$  decreases with increasing  $\Delta P_{H_2}$  due to hydrogen separation from the reaction void to the transport void. The decrease of  $x_{H_2}^A$  is related to  $K_{H_2}$  and is larger for membrane models with larger  $K_{H_2}$ . The total yield of H<sub>2</sub> is a result of the H<sub>2</sub> amount in both the reaction and transport voids.

## V. CONCLUSIONS

We have presented a simulation tool, termed the dual control cell reaction ensemble molecular dynamics (DCC-RxMD) method, to study fluid mixtures that are simultaneously chemically reacting and adsorbing in a porous material. The DCC-RxMD method was developed by coupling a nonequilibrium molecular dynamics method with two Monte Carlo based methods, namely, reaction ensemble Monte Carlo (REMC) and grand canonical Monte Carlo (GCMC). Control cells, which are in direct physical contact with the porous solid, are used to maintain the desired reac-

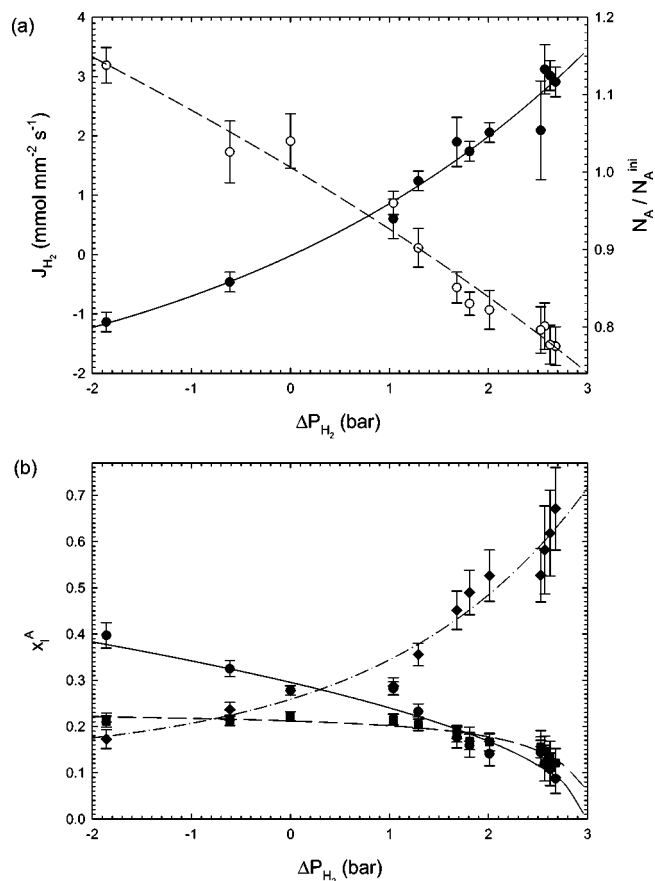


FIG. 8. (a) Hydrogen molar flux  $J_{H_2}$  (●) and  $N_A/N_A^{ini}$  (○) as a function of the hydrogen partial pressure difference  $\Delta P_{H_2}$ , and (b) the composition in the reaction void  $x_i^A$  (CH<sub>4</sub>, ■; H<sub>2</sub>, ●; CO, ◆) as a function of  $\Delta P_{H_2}$  in the case of PM2 obtained from the DCC-RxMD simulations. Due to identical initial compositions of CH<sub>4</sub> and CO<sub>2</sub>  $x_{CH_4}^A = x_{CO_2}^A$  within statistical uncertainties, therefore  $x_{CO_2}^A$  is not plotted. Lines serve as a guide to the eye only.

tion and flow conditions. The simulation setup closely mimics an actual experimental system in which the thermodynamic and flow parameters are precisely controlled. The method is akin to the dual control volume grand canonical molecular dynamics method that was developed to study the transport properties of fluid mixtures primarily in confined systems. The added feature of the DCC-RxMD method is the inclusion of chemical reactions, thus its applicability is to a wider range of processes beyond solely adsorption phenomena. The method presented here allows for the calculation of both equilibrium and nonequilibrium transport properties in porous materials such as diffusion coefficients, permeability, and mass flux. Effects on these properties due to the characteristics of the porous material can be predicted; characteristics such as the pore size distribution, connectivity, porosity, and surface area. Note that the DCC-RxMD method reduces to the RxMD method<sup>11</sup> if the REMC steps are performed in both control cells. Also note that in general, neither the DCC-RxMD nor the RxMD methods can provide reaction rate information but in turn, neither method is limited by reaction rates or activation energy barriers.

As an illustration of the method, we simulated the dry reforming of methane reaction within a nanoscale reactor model in the presence of a semipermeable membrane that

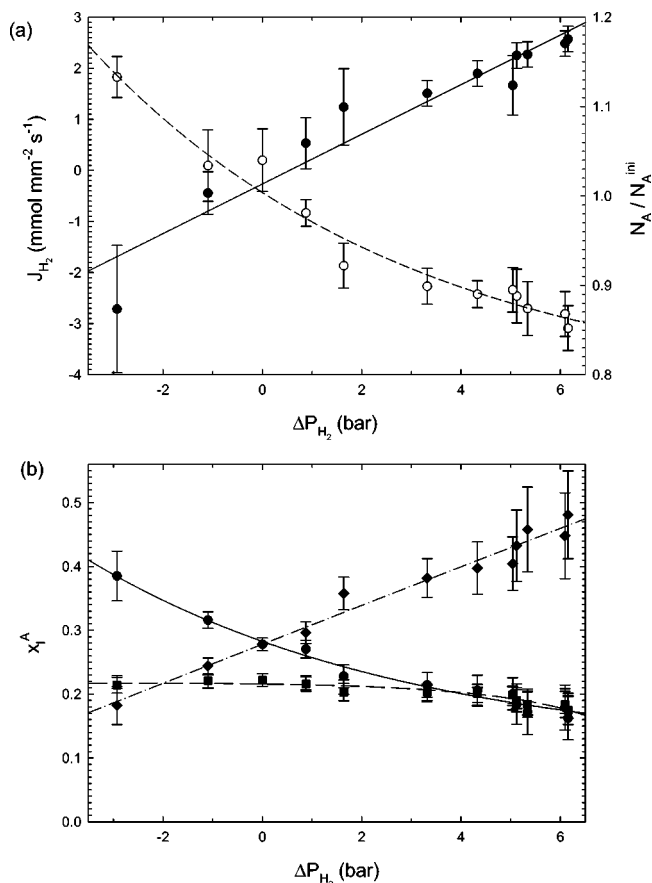


FIG. 9. (a) Hydrogen molar flux  $J_{H_2}$  (●) and  $N_A/N_A^{ini}$  (○) as a function of the hydrogen partial pressure difference  $\Delta P_{H_2}$ , and (b) the composition in the reaction void  $x_i^A$  ( $CH_4$ , ■;  $H_2$ , ●;  $CO$ , ◆) as a function of  $\Delta P_{H_2}$  in the case of RM obtained from the DCC-RxMD simulations. Due to identical initial compositions of  $CH_4$  and  $CO_2$   $x_{CH_4}^A = x_{CO_2}^A$  within statistical uncertainties, therefore  $x_{CO_2}^A$  is not plotted. Lines serve as a guide to the eye only.

was modeled as silicalite. We studied the effects of the membrane structure and porosity on the reaction species permeability by considering three different membrane models. We also studied the effects of an imposed pressure gradient across the membrane on the mass flux of the reaction species. The conversion of syngas ( $H_2/CO$ ) increased significantly in all the nanomembrane reactor models considered. An increase of 60% at the maximal imposed pressure occurred in the nanomembrane reactor model with a membrane that was exclusively permeable to  $H_2$ . The larger increase (80% and 150% at the maximal imposed pressures) occurred in the nanomembrane reactor models with membranes that exhibited larger values of  $H_2$  permeability but at the same time possessed very small yet undesirable permeabilities for the nonseparating components  $CH_4$ ,  $CO_2$ , and  $CO$ .

In the application of the DCC-RxMD method presented here, we considered membrane models that did not exhibit attractive character towards the reaction species. Further simulations that include effects of the relative adsorption behavior of the reaction species would be worthwhile. Here again such simulations could provide insight into the membrane characteristics that would most influence the conversion of reactants to products. Further, we note that analogous to the REMC method, multiple reactions can be simulated

simultaneously in the DCC-RxMD method; providing a means of studying systems in which competing reactions play a crucial role. Finally, we should note that in this study, the DCC-RxMD method was applied to a system where a semipermeable membrane exists between the reaction and transport voids. However, this could be any type of porous solid model, be it a simpler slitpore model<sup>21</sup> or a more realistic model such as an activated carbon.<sup>40</sup> Within the limit of the available computational resources, DCC-RxMD simulations could also include porous solids on a longer length scale such as microporous solids.

## ACKNOWLEDGMENTS

This research was supported by the Grant Agency of the Czech Republic (Grant No. 203/02/0805), by the Grant Agency of the Academy of Sciences of the Czech Republic (Grant No. IAA4072102), and by the National Research Council of Canada (Grant No. OGP 1041). J.K.B. gratefully acknowledges support from the National Research Council through the U.S. Army Research Laboratory. F.R.S. gratefully acknowledges the support from the MCyT in the program Ramón y Cajal.

- <sup>1</sup> *Beyond the Molecular Frontier. Challenges for Chemistry and Chemical Engineering*, edited by R. Breslow and M. V. Tirrell (National Academic, Washington, DC, 2003).
- <sup>2</sup> L. D. Gelb, K. E. Gubbins, R. Radhakrishnan, and M. Sliwinski-Bartkowiak, Rep. Prog. Phys. **62**, 1573 (1999).
- <sup>3</sup> C. H. Turner, J. K. Johnson, and K. E. Gubbins, J. Chem. Phys. **114**, 1851 (2001).
- <sup>4</sup> C. H. Turner, J. Pikunic, and K. E. Gubbins, Mol. Phys. **99**, 1991 (2001).
- <sup>5</sup> C. H. Turner, J. K. Brennan, J. K. Johnson, and K. E. Gubbins, J. Chem. Phys. **116**, 2138 (2002).
- <sup>6</sup> M. Borówko, A. Patrykiewicz, S. Sokołowski, R. Zagórski, and O. Pizio, Czech. J. Phys. **48**, 371 (1998).
- <sup>7</sup> M. Borówko and R. Zagórski, J. Chem. Phys. **114**, 5397 (2001).
- <sup>8</sup> W. R. Smith and B. Třiska, J. Chem. Phys. **100**, 3019 (1994).
- <sup>9</sup> J. K. Johnson, A. Z. Panagiotopoulos, and K. E. Gubbins, Mol. Phys. **81**, 717 (1994).
- <sup>10</sup> M. Lísal, I. Nezbeda, and W. R. Smith, J. Chem. Phys. **110**, 8597 (1999).
- <sup>11</sup> J. K. Brennan, M. Lísal, K. E. Gubbins, and B. M. Rice, Phys. Rev. E (in press).
- <sup>12</sup> A. Papadopoulou, E. D. Becker, M. Lupkowski, and F. van Swol, J. Chem. Phys. **98**, 4897 (1993).
- <sup>13</sup> K. K. Sirkar, P. V. Schanbhag, and A. S. Kovvali, Ind. Eng. Chem. Res. **38**, 3715 (1999).
- <sup>14</sup> G. S. Heffelfinger and F. van Swol, J. Chem. Phys. **100**, 7548 (1994).
- <sup>15</sup> J. M. D. MacElroy, J. Chem. Phys. **101**, 5274 (1994).
- <sup>16</sup> M. G. Martin, A. P. Thompson, and T. N. Nenoff, J. Chem. Phys. **114**, 7174 (2001).
- <sup>17</sup> G. Arya, H.-C. Chang, and E. J. Maginn, J. Chem. Phys. **115**, 8112 (2001).
- <sup>18</sup> M. P. Allen and D. J. Tildesley, *Computer Simulation of Liquids* (Clarendon, Oxford, 1987).
- <sup>19</sup> D. Frenkel and B. Smit, *Understanding Molecular Simulation: From Algorithms to Applications* (Academic, London, 2002).
- <sup>20</sup> A. Basile and L. Paturzo, Catal. Today **67**, 55 (2001).
- <sup>21</sup> D. Nicholson and N. G. Parsonage, *Computer Simulation and the Statistical Mechanics of Adsorption* (Academic, New York, 1982).
- <sup>22</sup> R. F. Cracknell, D. Nicholson, and N. Quirke, Phys. Rev. Lett. **74**, 2463 (1995).
- <sup>23</sup> D. J. Evans and G. P. Morris, *Statistical Mechanics of Nonequilibrium Liquids* (Academic, London, 1990).
- <sup>24</sup> D. J. Evans, W. G. Hoover, B. H. Failor, B. Moran, and A. J. C. Ladd, Phys. Rev. A **28**, 1016 (1983).
- <sup>25</sup> E. Enciso, N. G. Almarza, S. Murad, and M. A. Gonzalez, Mol. Phys. **100**, 2337 (2002).
- <sup>26</sup> D. Brown and J. H. R. Clarke, Mol. Phys. **51**, 1243 (1984).

- <sup>27</sup>B. M. Rice, W. Mattson, J. Grosh, and S. F. Trevino, *Phys. Rev. E* **53**, 623 (1996).
- <sup>28</sup>S. J. Stuart, A. B. Tutein, and J. A. Harrison, *J. Chem. Phys.* **112**, 6472 (2000).
- <sup>29</sup>W. R. Smith and R. W. Missen, *Chemical Reaction Equilibrium Analysis: Theory and Algorithms* (Wiley-Interscience, New York, 1982), reprinted with corrections (Krieger, Malabar, FLA, 1991).
- <sup>30</sup>M. W. Chase, Jr., NIST-JANAF Thermochemical Tables, 4th ed., *J. Phys. Chem. Ref. Data Monogr.* **9** (1985).
- <sup>31</sup>L. Xu, M. G. Sedigh, T. T. Tsotsis, and M. Sahimi, *J. Chem. Phys.* **112**, 910 (2000).
- <sup>32</sup>M. G. Sedigh, W. J. Onstot, L. Xu, W. L. Peng, T. T. Tsotsis, and M. Sahimi, *J. Phys. Chem. A* **102**, 8580 (1998).
- <sup>33</sup>M. Firouzi, T. T. Tsotsis, and M. Sahimi, *J. Chem. Phys.* **119**, 6810 (2003).
- <sup>34</sup>W. A. Steele, *The Interaction of Gases with Solid Surfaces* (Pergamon, Oxford, 1974).
- <sup>35</sup>J. G. Powles, S. Murad, and P. V. Ravi, *Chem. Phys. Lett.* **188**, 21 (1992).
- <sup>36</sup>M. G. Martin, A. P. Thompson, and T. M. Nenoff, *J. Chem. Phys.* **114**, 7174 (2001).
- <sup>37</sup>L. D. Gelb and K. E. Gubbins, *Langmuir* **15**, 305 (1999).
- <sup>38</sup>I. A. Park and J. M. D. MacElroy, *Mol. Simul.* **2**, 105 (1989).
- <sup>39</sup>D. M. Ford and E. D. Glandt, *J. Membr. Sci.* **107**, 47 (1995).
- <sup>40</sup>J. Pikunic, C. Clinard, N. Cohaut, K. E. Gubbins, J.-M. Guet, R. J.-M. Pellenq, I. Rannou, and J.-N. Rouzaud, *Proceedings of the Sixth International Symposium on the Characterization of Porous Solids*, edited by F. Rodriguez-Reinoso, B. McEnaney, J. Rouquerol, and K. K. Unger (Elsevier, Amsterdam, 2002), pp. 16–26.